INCEEUROPE

8th International Conference
on
Wind Turbine Noise
Lisbon – 12th to 14th June 2019

Analysis of a high fidelity aero-servo-elastic process chain to assess low-frequency emissions from wind turbines

Florian Wenz, IAG, University of Stuttgart, florian.wenz@iag.uni-stuttgart.de
Levin Klein, IAG, University of Stuttgart, levin.klein@iag.uni-stuttgart.de
Thorsten Lutz, IAG, University of Stuttgart, thorsten.lutz@iag.uni-stuttgart.de
Philipp Rettler, SWE, University of Stuttgart, rettler@ifb.uni-stuttgart.de

Summary

The increase in computational resources enables high fidelity simulations of wind turbines which allow to capture evermore phenomena including the acoustic low-frequency emissions. One of the remaining challenges is to verify these numerical results in the present study. A high fidelity process chain is used to numerically investigate the low-frequency emissions from a generic wind turbine. It consists of a computational fluid dynamics (CFD) solver coupled to a multi-body simulation (MBS) solver to take aeroelasticity into account and includes a controller for a realistic load behaviour. The sound pressure at discrete observer positions surrounding the turbine is calculated by means of a Ffowcs-Williams-Hawkings (FW-H) acoustic solver. A comparison with measurements requires an appropriate post-processing and visualisation of the sound pressure signal. Statistical analyses are often well-suited since the operational conditions and wind turbine geometries are in many cases not accurately reproduced in the simulation. However, discrete events like the blade-tower interaction can sometimes be better described by time series. A few different evaluation approaches are applied on the numerical results to show their suitability and significance. Especially, a variable rotational speed hampers the analysis in frequency domain and needs to be considered. The computational results of a generic wind turbine are qualitatively compared to acoustic low-frequency measurements of a commercial wind turbine to qualitatively verify the numerical process chain.

1. Introduction

There are a lot of publications about low-frequency emissions from wind turbines. Hubbard and Shepherd [1] are among the first to mention acoustic pulses due to the blade-tower interaction at blade-passing frequency (BPF) and its harmonics. Nowadays this interaction is considered to be the major cause of the low-frequency emissions from wind turbines based on measurements [2] [3] as well as simulations [4] [5]. Therefore, the major part of the low-frequency noise has the same origin and it is adequate to focus on the coherent part of the acoustic signal. Hessler et al. [6] give an overview over the latest findings in the field of low-frequency noise of wind turbines. The importance of correctly capturing the blade passing pulse of the blade-tower passage is

shown by Richarz et al. [7] who state that due to random phase shifts during propagation the inaudible low-frequency pulse can get audible. The local velocity and temperature gradients in a turbulent flow alter the local acoustic wave speed, when the length scale of the eddy and the acoustic wavelength are similar. This is mainly the case for higher harmonics which are otherwise masked by broadband noise but are enhanced in this way at an observer position.

1.1 Scope and Objectives

This paper addresses the blade-tower passage emission of wind turbines and the quality of its prediction with a numerical high-fidelity process chain. A CFD-MBS coupling [4] is used to run a complex wind turbine simulation including as many occurring effects as currently possible. More precisely, a generic 5 MW turbine with six flexible structures, namely, three blades, tower, foundation and drive train, is simulated. The included controller is forced to change pitch and rotation speed since a sheared turbulent inflow close to rated conditions is used. The acoustic pressure at defined observer positions is calculated based on the surface pressure using the FW-H equation. Afterwards the sound pressure time series is post-processed with different approaches. Depending on the operational conditions and the mechanism which are evaluated, their suitability and significance is shown with the focus on enabling comparisons to measurements.

2. Numerical Details

The low-frequency emissions from a generic 5 MW wind turbine are investigated numerically. The used high-fidelity process chain allows fully coupled CFD simulations under realistic turbulent inflow conditions including a pitch and rotational speed controller.

2.1 Numerical Process Chain

The simulation results were obtained using the high-fidelity process chain established by Klein et al. [4]. As described in this reference, the basis for the numerical simulations is the CFD solver FLOWer [8]. It is a compressible, dual time-stepping, block structured Reynolds-averaged Navier–Stokes (RANS) solver. The implemented CHIMERA technique allows the use of multiple grids for the structures and the background. The solver is continuously extended at the Institute of Aerodynamic and Gas Dynamics (IAG) [9], [10] improving its suitability for wind turbine simulations [11], [12]. The structural deformations are calculated with the commercial MBS solver SIMPACK [13] applying nonlinear beam theory.

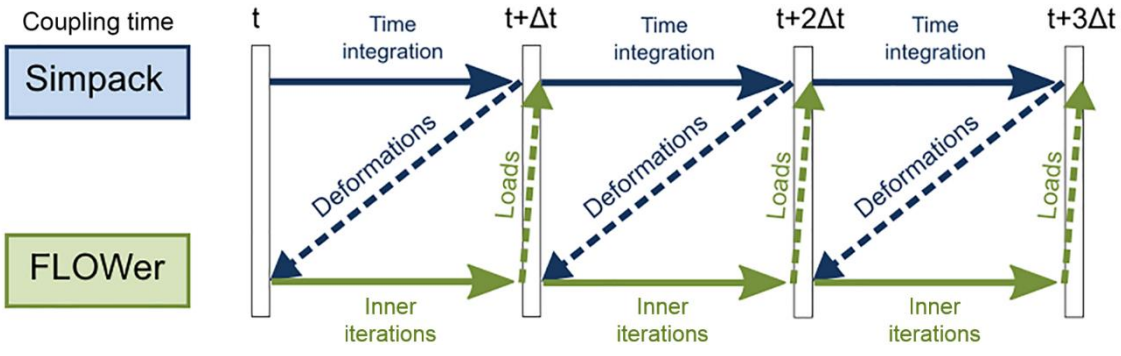

Figure 1: Explicit coupling scheme of the FLOWer–SIMPACK coupling *[4]*.

The coupling between FLOWer and SIMPACK enables combined calculation of rotating and non-rotating parts and allows to consider flexible deformations and rigid-body motions simultaneously. Hence, pitch motions and changes in rotational speed of the rotor caused by a variable speed collective pitch controller can be transferred from the MBS solver to the CFD solver. The employed coupling is a partitioned approach which uses an explicit coupling scheme depicted in

Figure 1. The communication is realized with 160 markers distributed over the turbine structures at which integrated loads and deformations are transferred. This fluid-structure interaction (FSI) takes the influence of unsteady structural deformation on the aerodynamics into account by deforming the CFD mesh.
The coupled FLOWer-SIMPACK simulations generate time series of the surface pressure distribution on the turbine. These are used to calculate the aeroacoustic signal at distant, predefined observer positions by means of the in-house FW-H solver ACCO. Volume sources generated by free-flow turbulence, ground reflections and nonlinear propagation due to atmospheric layering and turbulence are neglected. Hence, an undisturbed propagation and observers located in the acoustic far field are assumed.
For more information on the process chain in general and the implementation and functionality in detail please refer to Klein et al. [4].

2.2 Simulation Cases

The simulated turbine is derived from the generic 5 MW turbine developed by the National Renewable Energy Laboratory (NREL) [14], which was slightly modified in the OFFWINDTECH project [15]. The hub height is 90 m and the rotor diameter is 126 m. The rated conditions of the modified onshore configuration of the turbine are given with a rotational speed of 11.7 RPM at a hub wind speed of 11.3 ms^{-1}. The simulations without controller use rated rotational speed and the inflow conditions aim to meet rated wind speed at hub height. The atmospheric boundary layer (ABL) is represented by the power law with an exponent of 0.19. The generic atmospheric turbulence is generated using Mann's model [16] resulting a turbulence intensity at the turbine position of 16 %. Hence, a turbulent ABL inflow involves shear as well as turbulence.
The described numerical setup was used to investigate the impact of model complexity on the calculated low-frequency emissions by Klein et al. [4]. On top of these already presented cases the present paper shows results of a case with included controller and an additional degree of freedom, namely the drive train torsion. Overall, two different load cases (LC) and three different levels of fluid structure coupling (FSC) are considered. Table 1 summarises all simulation cases regarded hereafter.

Case name	Inflow	Flexible structures	Controller
LC2 [4]	uniform	none	no
LC2_FSC3 [4]	uniform	blades, tower, foundation	no
LC4_FSC3 [4]	turbulent ABL	blades, tower, foundation	no
LC4_FSC5	turbulent ABL	blades, tower, foundation, drive train	yes

Table 1: Definition of simulation cases.

2.3 Computational Setup

The CFD model is taken from Klein et al. [4]. It consists of 10 independent body meshes, namely three blades, tower, hub, nacelle, hub-nacelle connector and three blade-hub connectors, as well as a background mesh all connected via the CHIMERA technique. The resolution of the body meshes allows to fully resolve the boundary layer ($y^+ \leq 1$) and the background mesh is refined upstream of the turbine to propagate the atmospheric turbulence. Overall, the mesh consists of 86 million cells. The unsteady RANS simulations are performed using a second-order dual time-stepping scheme according to Jameson [17]. A physical time step corresponding to 0.75° azimuth (≈0.01068s) with 100 inner iterations is applied for the evaluated part of the simulations. The spatial discretization in body meshes is based on second-order central discretization with Jameson–Schmidt–Turkel (JST) artificial dissipation term [18]. The fifth-order WENO scheme is applied in the background mesh in order to reduce the dissipation of vortices. All simulations are fully turbulent and use the k-ω-SST model by Menter [19] for turbulence modelling.
The structural model in SIMPACK was built by Matha et al. [20]. The blades and the tower are each represented by multiple flexible bodies so that they are modelled nonlinearly, whereas hub, nacelle and foundation are kept rigid. The foundation is connected to the ground with a spring-

damper system [4]. In simulations with controller the drive train is also flexible with respect to torsion.

3. Evaluation of Simulation Results

The sampling rate of the sound pressure is equal to the physical time step of the simulations Δt=0.01068 s. Thus, the highest captured frequency is 46.8 Hz. However, the spatial resolution at the source, i.e. the surface mesh of the turbine, also limits the highest resolved frequency. The shortest wavelength properly simulated is limited by the largest surface cells. Assuming it takes ten cells to properly capture a pressure wave, the highest frequency to be well resolved is approximately 25Hz. All depicted sound pressure levels are unweighted and the time signals are cut to multiples of blade passages before evaluation.

3.1 Methods for Evaluation of Acoustic Data

Merchant et al. [21] give a good overview on approaches and techniques to evaluate acoustic signals statistically as well as in the time domain. In general the sound pressure is measured in Pascals (Pa). However, it is usually expressed as sound pressure level (SPL) in decibels (dB) due to the huge pressure range which is audible

$$\mathrm{SPL_{rms}} = 20 \cdot \log_{10}\left(\frac{\mathrm{p_{rms}}}{\mathrm{p_0}}\right) \mathrm{dB}.$$

The standard reference sound pressure for airborne sound p_0=20 μPa is used in this paper. The sound pressure p used for decibel calculation is expressed in root-mean-square values. This means the effective sound pressure is evaluated as it is defined in IEC 103-02-03. A single value results from this evaluation. It represents the broadband sound pressure level within a given time interval including all captured frequencies. This is the most often used average acoustic metric. However, this approach gives no information on the characteristic of the sound like peak sound level or tonality and does not allow to specifically evaluate the low-frequency emission. Therefore, more substantial evaluation methods need to be applied.

A typical approach to analyse acoustical data is a transformation into the frequency domain to gain insight into the frequency characteristics. This is normally done using Fast-Fourier-Transformation (FFT). The spectral sound pressure level is calculated using

$$\mathrm{SPL(f)} = 20 \cdot \log_{10}\left(\frac{\frac{2}{\sqrt{2}} \cdot \left|\frac{\mathrm{FFT[p(t)]}}{\mathrm{L}}\right|}{\mathrm{p_0}}\right) \mathrm{dB},$$

where L is the number of samples in the pressure signal p(t). The frequencies above the Nyquist frequency $F_s/2$ are discarded and hence the remaining frequency bins are doubled to get the single-sided FFT. Since the pressure signal is considered to be a superposition of sine waves it is divided by $\sqrt{2}$ to get the effective sound pressure level.
However, for not entirely periodic signals the interpretation of the resulting spectra with regard to the coherent component is difficult. Vanderkooy and Mann [2] introduce an approach to regularize quasi-periodic acoustic signals of wind turbines with varying rotational speed and obtain periodic data which are better suited for a FFT evaluation. The necessary information on the blade passage period is extracted from the original sound pressure signal by detecting local peaks. The duration of the original signal is than divided by the number of blade passages captured in the signal. The obtained mean blade passage period is discretised equidistantly so that the original sampling rate is roughly obtained. Each of the detected blade passage periods

is interpolated on one of the normalised mean blade passage periods. The string of these segments is the resampled signal with a warped time line.
For strongly time-dependent sound pressure signals the short-time Fourier transform (STFT) is a method of Fourier analysis to also detect the temporal change in the frequency spectrum. The time signal is divided into multiple segments which are individually transferred into the frequency domain using FFT. The changing spectra are visualised as a function of time in spectrograms. This method combines evaluation in the frequency domain and time domain and hence a trade-off between frequency resolution and time resolution is necessary. Overlapping time windows can be used to smooth the data in the time domain.
If the sound has a rather impulsive character evaluating the pressure waveform directly in the time domain is a good option. Vanderkooy and Mann [2] investigated the shape of the coherent acoustic blade passing pulse of multiple turbines which can be used as reference for simulation results. The shape of the acoustic pulse is often masked by background noise of different sources. Therefore, an approach is to reconstruct the signal by inverse transforming the first couple of BPF harmonics extracted from the spectrum.

3.2 Analysis of Average Values

The broadband root-mean-square sound pressure level SPL_{rms} is evaluated using the FW-H solver at a carpet of 3600 observers on the ground surrounding the turbine. The highest included frequency is, as already mentioned, 46.8 Hz and the evaluated signals have a duration of seven (LC2) and nineteen revolutions (LC4_FSC5), respectively. The outermost circle of observers has a radius of 2000 m. In Figure 2 and Figure 3 the noise carpets for the cases LC2 and LC4_FSC5 (compare Table 1) are shown. These plots are well suited to get information on the directivity of the acoustic low-frequency emission and its total level.

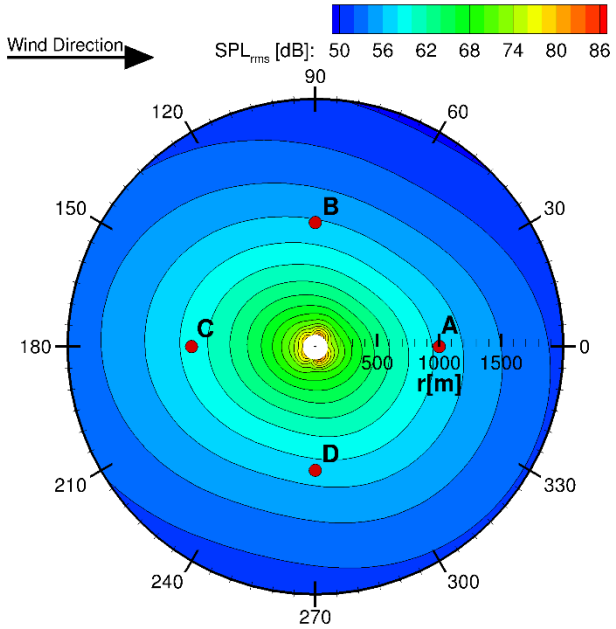

Figure 2: Unweighted broadband SPL (f<46.8 Hz) on the ground for case LC2.

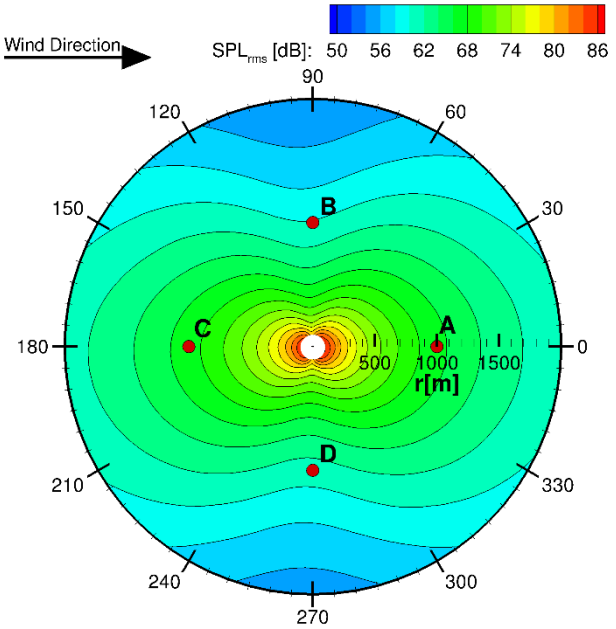

Figure 3: Unweighted broadband SPL (f<46.8 Hz) on the ground for case LC4_FSC5.

The sound pressure level for case LC4_FSC5 is significantly higher and the directivity is also slightly different. Since there are multiple levels of complexity between these two cases, looking at the intermediate cases helps to identify the causes. The values at four discrete observers A-D, each at a distance of 1000 m from the turbine, of all four cases are compared in Table 2.
As expected and already found by Klein et al. [4] the SPL is increased when deformation is considered. The main reason for that was identified as the decreased blade-tower distance [22]. Adding turbulence to the inflow further increases the SPL but only in upstream and downstream

direction. The impact of the controller is rather small. Certainly, the resulting strong directivity for such low-frequencies is an interesting finding. However, looking at these plots and values, it cannot be decided whether the increase in magnitude is due to more broadband noise or to higher tonal peaks. Generally, it is not possible to gain information about the character of the sound. Moreover, these values include also the energy of frequencies which might not be correctly resolved in the simulation because of the above mentioned mesh limitations. To get more insight an evaluation in the frequency domain is necessary.

Observer	LC2	LC2_FSC3	LC4_FSC3	LC4_FSC5
A	57.5	64.2	66.5	66.6
B	56.3	61.7	61.3	60.2
C	58.8	65.2	67.2	67.2
D	57.0	62.2	62.0	61.1

Table 2: Unweighted SPL_{rms} in dB (f<46.8 Hz) at discrete observers 1000 m from the turbine for all cases.

3.3 Analysis in Frequency Domain

Performing a Fast-Fourier-Transform of the sound pressure signal at discrete observer positions allows to analyse the frequency characteristic. The signal is cut into multiples of the blade passage to obtain an almost periodic input to the FFT. This approach was already used by Klein et al. [4] to evaluate the cases LC2, LC2_FSC3 and LC4_FSC3. The key observation was that the acoustic emission occurs mainly at the BPF and its harmonics. Moreover, it was found that the reduced blade-tower distance when considering flexibility increases the peak levels and turbulent inflow increases the broadband level. All these observations could be made by directly transforming the pressure signal with a FFT to the frequency domain.

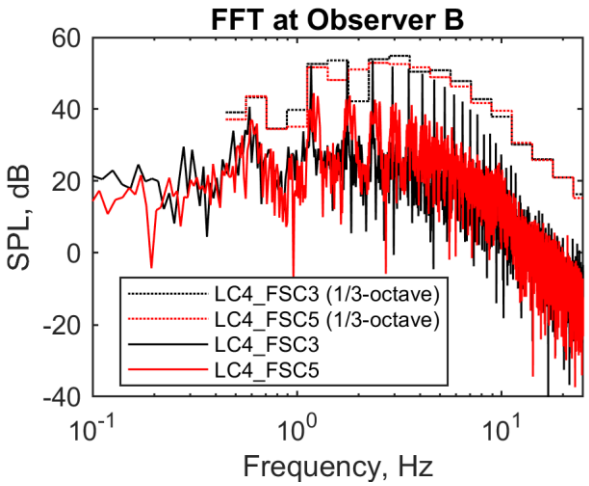

Figure 4: Spectra of unweighted SPL for cases LC4_FSC3 and LC4_FSC5 at observer B.

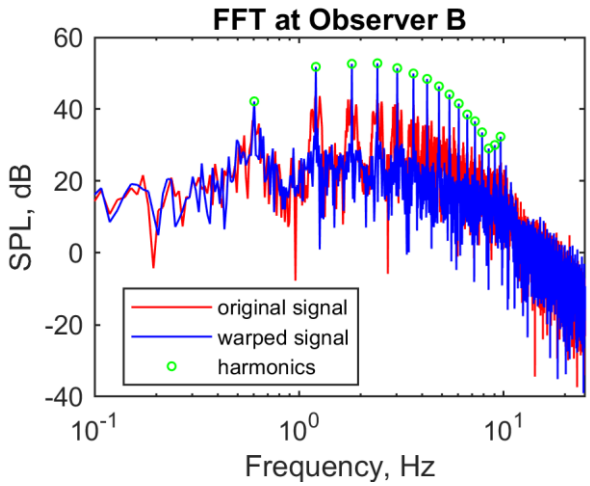

Figure 5: Spectra of unweighted SPL for case LC4_FSC5 at observer B of original and warped signal.

This approach yields meaningful results if the input signal is periodic which is given for all cases with constant rotational speed. However, the spectrum of the case LC4_FSC5, with a variable rotational speed, shown in Figure 4, has a significantly different shape. The issue is whether the difference has a real physical cause or is the consequence of an inappropriate evaluation? An indication that the low frequency emissions of the cases are actually very similar are the almost identical one-third octave band SPLs (see Figure 4). Since the requirement for a FFT of a periodic input signal is violated the differences are most likely caused by the evaluation approach. To confirm this, the time warp, described in section 3.1, is applied. The results are plotted in Figure 5 in comparison to the FFT of the unaltered signal.

The spectrum of the reconstructed periodic signal shows, as expected, very clearly the fundamental frequency and its harmonics. Now the spectrum is very similar to, for example, the one of case LC4_FSC3 in Figure 4. Therefore, it can be concluded that also in the case with controller the blade-tower interaction is the dominant acoustic source in the regarded frequency range. To verify that the controller did not alter the SPL caused by the blade passage, the SPL of the first 15 harmonics (exemplarily marked in Figure 5) are added up in Table 3.

	LC2	LC2_FSC3	LC4_FSC3	LC4_FSC5
SPL_{15harm} [dB]	56.1	61.7	60.7	59.8
% of SPL_{rms}	99.6	99.9	99.0	99.3

Table 3: Unweighted SPL of first 15 harmonics in dB at observer B and its ratio of SPL_{rms} (f<46.8 Hz) for all cases.

For all cases more than 99 % of the SPL_{rms} (f<46.8 Hz) is caused by the first 15 harmonics of the BPF. This evaluation is not possible for cases with varying rotational speed without reconstructing a periodic signal since otherwise the harmonic series is not clearly extractable (see Figure 5). It can also be seen that adding turbulence to the inflow reduces the ratio slightly compared to uniform inflow. This corresponds well with the observation of an increase in broadband noise.
Despite the advantages of the signal warping for frequency analyses, this evaluation method distorts the real character of the acoustic signal, especially if the blade passage period varies strongly. This is because the method is a kind of averaging and the time information gets lost. The mentioned STFT and a visualisation via spectrograms preserves the time information, namely the variations over time (see Figure 6).

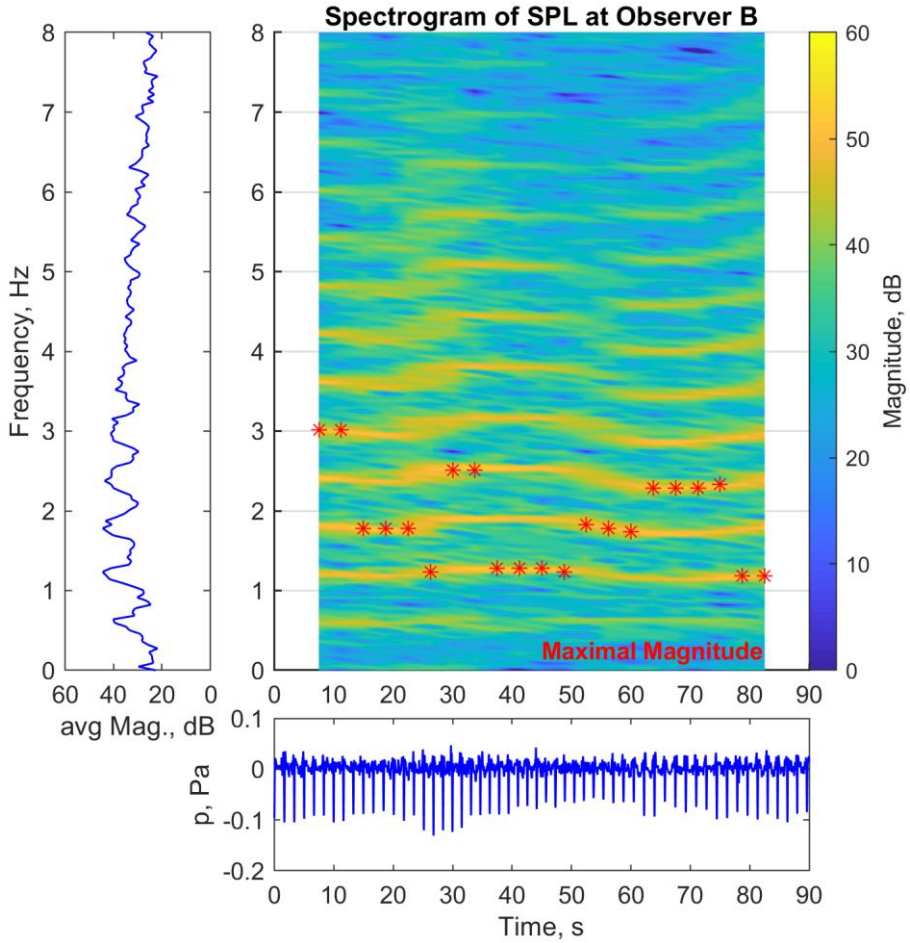

Figure 6: Spectrogram of case LC4_FSC5 at observer B.

The shown spectrogram was created with a window size of 15 s and a hop size of 3.75 s, resulting in 75 % overlap of the frames. A rectangular window was applied. The plot on the left

of the figure is created by averaging the magnitude of the spectrogram for each frequency. The BPF and its harmonics are well visible and the magnitudes correspond to the findings in Figure 5 for the warped signal. Even though the BPF itself has rather low amplitudes, looking at its harmonics the increase of rotational speed at about 30 s as well as the decrease at approximately 60 s is obvious. The included red markers depict the maximal magnitude for each window. The maximal SPL value varies between 49.3 dB and 53.3 dB what is in accordance with the peaks in the FFT plots. Moreover it can be seen that the maximum jumps between the second and the fifth harmonic of the BPF.

3.4 Analysis in Time Domain

All the evaluations shown so far indicate that the blade-tower passing is the dominant event for acoustic low-frequency emissions. Although this is a periodically occurring event and can, as shown, be evaluated in the frequency domain, the passage itself is a fairly impulsive sound. Therefore, looking at the pressure waveform allows some interesting observations as well as enable another way to compare simulation and measurement. In Figure 7 the warped pressure signal of case LC4_FSC5 is plotted for observers B and C. At the side of the turbine, namely observer B, the blade passing is very prominent (upper graph). Downstream of the turbine (observer C), however, the blade passing is almost not visible since many fluctuations are superposed (lower graph). This is because the turbulent inflow interacts with the blades which emit mainly in upstream and downstream direction (see Klein et al. [4]). Hence to visualise the shape of the blade passing pulse at observer C the pressure signal is reconstructed using the first 15 harmonics (marked in Figure 5). Now a clear pulse is visible, even though it is significantly different than at observer B. Comparable differences in the shape of coherent blade passing pulses extracted from measurements of different wind turbines were also observed by Vanderkooy and Mann [2].

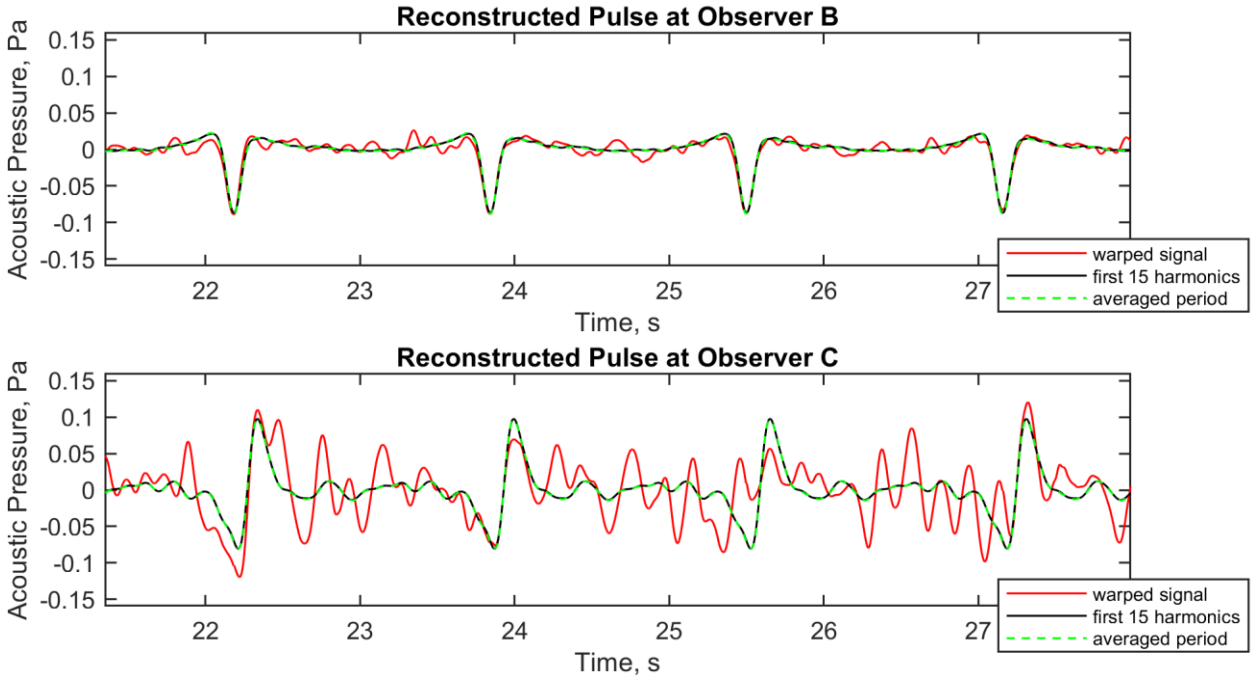

Figure 7: Pressure signal of case LC4_FSC5, reconstructed signal using 15 harmonics and averaged periods.

Another interesting finding made by Vanderkooy and Mann [2] is that averaging all periods removes most of the noise and only the blade passing pulse remains. This is also true for the simulation results of case LC4_FSC5 and confirms that the broadband noise is of stochastic nature and has no tonal components, leaving the blade tower interaction as only source of low-frequency tonality.

4. Qualitative Comparison with Measurements

The simulation results shown so far match the expectations and reasonable explanations could be found for the observations. Still at least a qualitative comparison to measurements is essential to verify the numerical process chain and its results. Obviously, there are no measurements for a generic wind turbine. Therefore, absolute values cannot be verified, but the relative values of peaks in FFTs as well as the shape of the spectrogram and the blade passing pulse can be compared. The measurements shown in this paper were carried out by Stuttgart Wind Energy (SWE) of the University of Stuttgart by using the procedure explained in [23]. A GRAS 47AC free-field infrasound microphone with a frequency range from 0.09 Hz to 20 kHz (±3 dB) was used. It was placed in a distance of about 140 m southeast (125°) of a single multimegawatt wind turbine. During the evaluated period of the measurement the wind came from a direction of 145°-180° with a velocity of about 5 ms^{-1} at hub height. Hence, the microphone was placed more or less upstream of the turbine. Since the numerical results indicate that the acoustic emission is similar in upstream and downstream direction a qualitative comparison with observer C is reasonable.
Figure 8 shows the spectrum of a 400 s interval of the measured acoustic pressure. Before the FFT was performed the sampling rate was reduced to 100 Hz resulting in 50 Hz to be the highest resolved frequency. A period with relatively constant wind speed and hence constant rotational speed was chosen. As for the simulation results, discrete peaks occur which can be linked to the BPF and its harmonics. Again not the BPF itself but a higher harmonic has the highest amplitude. The first 15 harmonics contain 84 % of the SPL_{rms} (f<50 Hz). This ratio is considerably lower than for the simulations, but the measured signal also contains background noise sources not related to the wind turbine.

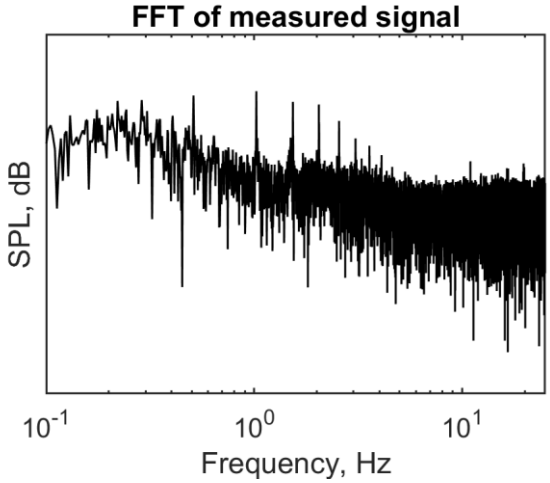

Figure 8: Spectrum of unweighted SPL of measured sound pressure.

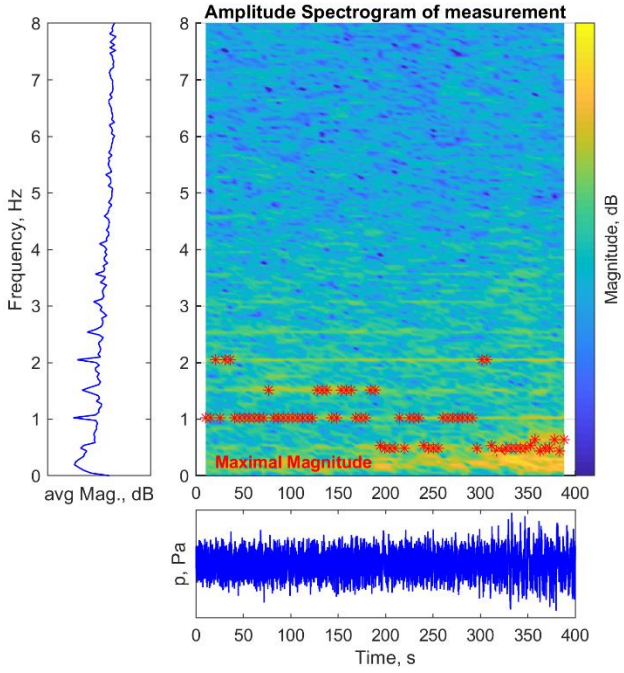

Figure 9: Spectrogram of measured acoustic pressure.

Looking at the spectrogram in Figure 9, narrow lines with higher magnitudes are visible. These represent the BPF and its harmonics. The lines are almost straight confirming that the rotational speed was indeed almost constant. As for the simulation, the maximal amplitude jumps between the harmonics. Overall, the first seven harmonics are visible in the plot on the left in Figure 9 showing the time-averaged SPL per frequency. This is less than in the simulation, but it should be noted that the dimensions of the simulated and measured wind turbine are significantly different and the wind speed was much lower in the measurement. In addition, an increase in amplitude is evident below 1 Hz starting after about 300 s whereas the higher harmonics continue unaltered. This suggests the presence of not turbine-related sound sources in the signal.

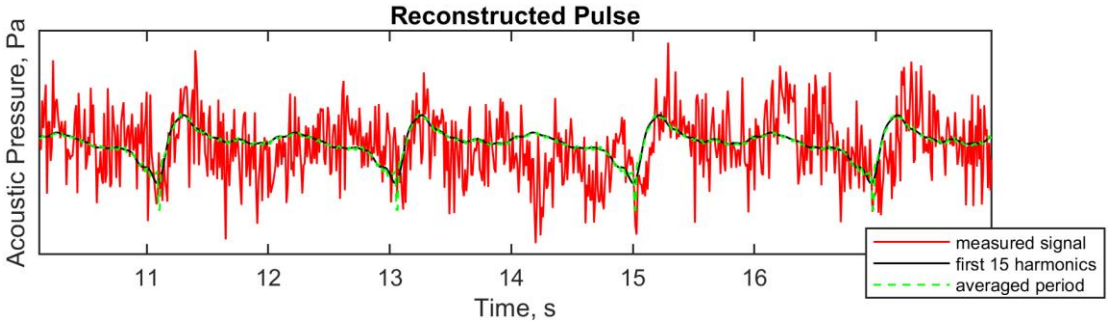

Figure 10: Measured pressure signal, reconstructed signal using 15 harmonics and averaged periods.

The reconstructed coherent pulse is depicted in Figure 10 in comparison to the original signal. Again in the signal itself the blade passing is hard to detect. The reconstructed waveform has an evident similarity with the pulse of the simulation at observer C (Figure 7 bottom). This is an indication that the simulation captures the blade-tower passage accurately.
Overall, the evaluation of the measured acoustic pressure shows similar phenomena as the simulation results and hence the process chain is able to capture the main effects contributing to the low-frequency emission from wind turbines.

5. Conclusions

The results of simulations with differing complexity performed by Klein et al. [4] are compared by means of different evaluation methods. The general directivity of the emission can be represented using the root-mean-square SPL evaluated at multiple observer positions. As long as the rotational speed is constant the character of the low-frequency emissions can be well visualised with a FFT. The tonality at the BPF and its harmonics is the dominant characteristic. When the rotational speed varies during the evaluation interval the FFT no longer reveals the tonality that clearly. A time warping must be applied or a spectrogram must be used to visualise the prominence of discrete frequencies. The reconstructed coherent pulse shows the general waveform of the blade-tower passage. The shape changes according to the observer position.
Some simulation results could be qualitatively confirmed by applying the same evaluation methods on a measured sound pressure. However, a final verification of the numerical process chain is only possible by simulating the commercial wind turbine at the same operational conditions as during the measurement. This would also allow to quantitatively validate the simulation results.

Acknowledgment

The studies were conducted as part of the joint research project “Objective Criteria for Seismic and Acoustic Emission of Inland Wind Turbines (TremAc), FKZ 0325839A”, funded by the German Federal Ministry for Economic Affairs and Energy (BMWi). The authors are grateful for the financial support. The authors gratefully acknowledge the High-Performance Computing Center Stuttgart (HLRS) for providing computational resources within the project WEALoads.

References

[1] H. H. Hubbard and K. P. Shepherd, “Aeroacoustics of large wind turbines,” *The Journal of the Acoustical Society of America,* vol. 89, no. 6, pp. 2495-2508, 1991.

[2] J. Vanderkooy and R. Mann, “Measuring wind turbine coherent infrasound,” in *International Conference on Wind Turbine Noise*, Glasgow, 2015.

[3] K. L. Hansen, B. Zajamsek and C. H. Hansen, “The Occurrence of Nocturnal Wind Farm Rumbling Noise,” in *7th International Conference on Wind Turbine Noise*, Rotterdam, 2017.

[4] L. Klein, J. Gude, F. Wenz, T. Lutz and E. Krämer, “Advanced computational fluid dynamics (CFD)–multi-body simulation (MBS) coupling to assess low-frequency emissions from wind turbines,” *Wind Energy Science,* no. 3, pp. 713-728, 2018.

[5] Y. Yauwenas, B. Zajamšek, J. Reizes, V. Timchenko and C. J. Doolan, “Numerical simulation of blade-passage noise,” *The Journal of the Acoustical Society of America,* vol. 142, p. 1575–1586, 2017.

[6] G. Hessler, G. Leventhall, P. Schomer and B. Walker, “Health Effects from Wind Turbine Low Frequency Noise & Infrasound Do Wind Turbines Make People Sick? That is the Issue,” *Sound and Vibration,* vol. 51, no. 1, pp. 34-44, 2017.

[7] W. Richarz and H. Richarz, “Propagation Through A Turbulent Atmosphere Makes Blade Passage Harmonics Audible,” in *7th International Conference on Wind Turbine Noise*, Rotterdam, 2017.

[8] N. Kroll, C.-C. Rossow, K. Becker and F. Thiele, “The MEGAFLOW project,” *Aerospace Science and Technology,* vol. 4, no. 4, pp. 223-237, 2000.

[9] U. Kowarsch, M. Keßler and E. Krämer, “High order CFD-simulation of the rotor-fuselage interaction,” in *39th European Rotorcraft Forum*, Moscow, 2013.

[10] P. Weihing, J. Letzgus, G. Bangga, T. Lutz and E. Krämer, “Hybrid RANS/LES capabilities of the flow solver FLOWer-application to flow around wind turbines,” in *The 6th Symposium on Hybrid RANS-LES Methods*, Strassbourg, 2016.

[11] K. Boorsma, J. Schepers, S. Gomez-Iradi, I. Herraez, T. Lutz, P. Weihing, L. Oggiano, G. Pirrung, H. Madsen, W. Shen, H. Rahimi and P. Schaffarczyk, “Final report of IEA Task 29, Mexnext (Phase 3),” IEA, ECN, Petten, the Netherlands, 2018.

[12] N. Sørensen, N. Garca, S. Voutsinas, E. Jost and T. Lutz, “Aerodynamics of Large Rotors WP2 Deliverable 2.6 Effects of complex inflow for the AVATAR reference rotor and NM80 rotors,” Technical Report, Petten, the Netherlands, 2017.

[13] SIMULIA, “Simpack Multi-Body Simulation Software,” Dassault Systèmes, [Online]. Available: http://www.simpack.com/.

[14] J. Jonkman, S. Butterfield, W. Musial and G. Scott, “Definition of a 5-MW reference wind turbine for offshore system development,” National Renew. Energ. Lab.(NREL), Golden, CO, United States, 2009.

[15] D. Bekiropoulos, T. Lutz, J. Baltazar, O. Lehmkuhl and N. Glodic, “D2013-3.1: Comparison of benchmark results from CFD-Simulation,” Deliverable report, KIC-OFFWINDTECH, 2013.

[16] J. Mann, “The spatial structure of neutral atmospheric,” *J. Fluid Mech.,* vol. 273, p. 141–168, 1994.

[17] A. Jameson, “Time dependent calculations using multigrid, with applications to unsteady flows past airfoils and wings,” in *10th Computational Fluid Dynamics Conference*, 1991.

[18] A. Jameson, W. Schmidt and E. Turkel, “Numerical solution of the Euler equations by finite volume methods using Runge Kutta time stepping schemes,” in *14th fluid and plasma dynamics conference*, 1981.

[19] F. R. Menter, “Two-equation eddy-viscosity turbulence models for engineering applications,” vol. 32, no. 8, pp. 1598-1605, 1994.

[20] D. Matha, S. Hauptmann, T. Hecquet and M. Kühn, “Methodology and results of loads analysis of wind turbines with advanced aeroelastic multi-body simulation,” in *DEWEK*, Bremen, 2010.

[21] N. D. Merchant, K. M. Fristrup, M. P. Johnson, P. L. Tyack, M. J. Witt, P. Blondel and S. E. Parks, “Measuring acoustic habitats,” *Methods in Ecology and Evolution,* vol. 6, no. 3, pp. 257-265, 2015.

[22] C. Hansen, B. Zajamšek and K. Hansen, “Infrasound and Low-Frequency Noise from Wind Turbines,” in *3rd Symposium on Fluid-Structure-Sound Interactions and Control*, Perth, 2015.

[23] F. Calarco, P. W. Cheng, T. Zieger and J. Ritter, “Acoustic and seismic emissions from wind turbines,” in *German Wind Energy Conference DEWEK*, Bremen, 2017.